LA-5257

Determination of the EMP Enhancement Factor

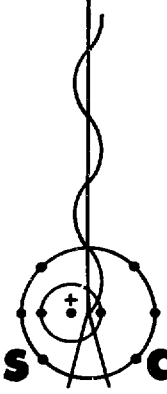

los alamos
scientific laboratory
of the University of California
LOS ALAMOS, NEW MEXICO 87544

UNITED STATES
ATOMIC ENERGY COMMISSION
CONTRACT W-7405-ENG. 36

Printed in the United States of America. Available from
National Technical Information Service
U. S. Department of Commerce
5285 Port Royal Road
Springfield, Virginia 22151
Price: Printed Copy $3.00; Microfiche $0.95

los alamos
scientific laboratory
of the University of California
LOS ALAMOS, NEW MEXICO 87544

LA-5257
UC-34
ISSUED: July 1973

Determination of the EMP Enhancement Factor

by

C. U. Benton
A. N. Phillips
R. W. Buchanan*
H. M. Fowles*

*Present Address: Denver Research Institute
University of Denver
Denver, Colorado

DETERMINATION OF THE EMP ENHANCEMENT FACTOR

By

C. U. Benton, A. N. Phillips,
R. W. Buchanan, and H. M. Fowles

ABSTRACT

EMP signals recorded aboard a C-135 aircraft are discussed with respect to the difference in amplitude and phase characteristics from that of a free-space signal. The enhancement factor is defined as the ratio of the normalized amplitude of the aircraft signal to the normalized amplitude of close-in sensors for a 2 MV pulsed antenna system. Three different close-in sensors were used to measure fields in excess of 10 kV/m. The radiation pattern was mapped in azimuth and elevation by the aircraft and the close-in sensors. The enhancement factor and the time rate of change of the EMP signal is seen to vary significantly with aircraft attitude and position.

I. INTRODUCTION

EMP-type signals recorded aboard aircraft differ from the free-space signal in amplitude and phase. In general, the amplitude of the EMP signal is greater than the free-space signal and a time or phase variation is seen over at least the first 100 ns or so when compared to a free-space signal.

Two wideband EMP sensor systems were calibrated in the Los Alamos Scientific Laboratory (LASL) parallel plate transmission line facility. The $\bar{E}$ field in this facility is known to within 1%. One system was installed on top of a C-135 aircraft at station 1070, and another on the bottom of the aircraft at station 1310.

The 2-MV pulsed antenna system of the Denver Research Institute (DRI) was installed in Hawaii. The radiated field was mapped using the DRI sphere sensor to determine the lobe bearing between 210° through 340° true from the pulser in azimuth, and from 1° to 52° in elevation. Two flights of the aircraft were made through the mapped portion of the radiated lobe.[1,2] Three close-in sensors in fixed locations simultaneously recorded the series of pulses observed by the aircraft for these flights.

Cross calibration of the two aircraft and the three close-in sensors was performed at the LASL facility after the operation. Analysis of the data in the time and frequency domains gave enhancement factors (E_f) that varied from 1.76 to 2.96 for the aircraft's bottom antenna (BA), and from 1.12 to 2.53 for the top antenna (AD). For the time from the first positive peak of the signal, the BA time varied from 30.3 to 49.3 ns, the AD time varied from 18.9 to 34.9 ns, compared to the DRI close-in sphere sensor time of 34.5 ns ± 2%. Plots of E_f vs bearing of the pulser from the aircraft, and E_f vs depression angle of the pulser from the aircraft, indicate the dependence of E_f on the direction of arrival of the EMP ray. A relationship between the time or phase anomaly to the elevation angle is also seen.

II. THE EMP SIMULATOR

The DRI pulsed antenna system (EMP simulator)[3] used to provide the source test function is a Marx generator, biconic antenna combination operated in the vertical mode. The Marx generator consists of 32 0.01 μF capacitors charged to a potential of 45 kV. These are then discharged into the antenna in series giving a source voltage at the antenna of 1.44 MV.

For purposes of this experiment, a vertically polarized signal was required. Further, ideally the signal should be uniform in azimuth and elevation profiles. Thus, a vertical monopole antenna is a better radiator than the biconic antenna. The simulator was modified before the experiment to eliminate as much of the lower bicone as possible. Ideally, the feed-point, which is a pressurized spark gap, would be composed of the radiating antenna element and a flat ground plane. Because of the main gap configuration, this was not completely realizable. However, the major portion of the bottom cone was removed and a ground plane installed, which left an effective bottom cone of about 12 in.

The simulator was installed in a 24-in.-deep pit which allowed the addition of an essentially flat ground plane in the immediate vicinity. The simulator modification and installation were important factors in the generation of a radiation pattern that was well behaved both in azimuth and elevation.

The simulator was installed at Lat. 21°19'50.8" and Long. 157°57'06". The installation site was composed of crushed coral at an elevation of about 2 ft above mean sea level. A ground plane was installed from an azimuth of 210°T to 340°T. The ground plane consisted of No. 8 aluminum wires at 3° increments and nominally 100 ft in length. The ground plane was extended to 160 ft in length from 230°T to 242°T to carry over a drainage ditch. This was an important sector since it extended in the direction of the DRI sphere sensor. The ground plane and pattern radiated in azimuth is shown in Fig. 1.

Three types of sensors were used to monitor the simulator output for control and field mapping. The first was a LASL parallel plate $\bar{E}$-field sensor which was located on the 292° azimuth at an elevation angle of 9.624° and at a slant distance of 47.188 m from the simulator.

The second sensor was a $\dot{B}$ loop located on the 242° azimuth at an elevation angle of 1.468° and at a slant distance of 72.573 m from the simulator.

The third sensor was the DRI sphere located on the 236° azimuth at an elevation angle of 8.726° and at a slant distance of 75.12 m from the simulator. The sphere sensor is self-contained, presents the smallest possible distortion of the $\bar{E}$ field, and is easily moved from position to position; thus, it was used for field mapping and cross-correlation of the other sensors.

The azimuthal field mapping was done using the sphere mounted on a forklift. It was recognized at the time that the forklift would prevent precise measurements after the first 10 ns; however, the peak field could be determined with confidence. The sensor antenna load gap was a nominal 22 ft 10 in. above the ground and the distance from the simulator was 100 ft, except for the points at 230°T and 239°T where the distance was 160 ft. Measurements were made at 14 points in 9° azimuthal increments from 212°T to 332°T. The $\dot{B}$ loop was used as control and two signals were recorded at each point.

The elevation radiation pattern was mapped using the sphere and the same $\dot{B}$ control. The sphere was supported by a crane with a 70-ft boom at a radial distance of 15.24 m from the simulator. Two measurements were made at 5° increments from 5° to 50° and a final reading was made at 52°. The radiated pattern in elevation should be a cosine function. Figure 2 shows the theoretical and measured radiation pattern in elevation.

III. CLOSE-IN SENSORS

The $\dot{B}$ sensor used was the standard model MGL 2A manufactured by EG&G. Its output was recorded on 35-mm film from a HP-183 oscilloscope.

The parallel plate $\bar{E}$-field sensor was built by LASL for this experiment. It consists of two small circular parallel plates approximately 5 in. in diameter and separated by

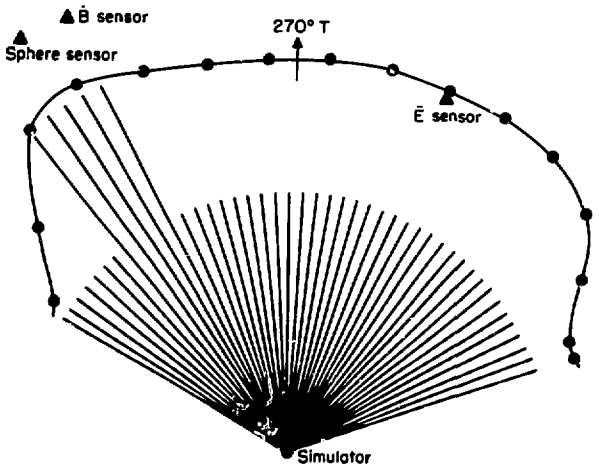

Fig. 1
Ground plane and azimuth field.

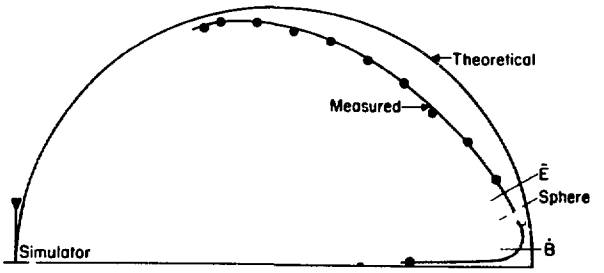

Fig. 2
Vertical field.

about 1 in. Between the plates are installed 500 MHz bandwidth amplifiers. Shielded leads carry the total output signal and input power 27 ft away and in the direct line-of-sight from the simulator.

The DRI sphere is a complete instrument package contained within a 25-in.-diam spherical shell. A radially mounted stub antenna serves as the electric field sensor.

The sensor was designed to occupy as small a volume as possible and have a simple geometrical shape so that any field distortion caused by the sensor could be readily calculated and accounted for. Other design criteria followed were electrical shielding of the recording instrumentation from the intense fields being measured and construction of the system as a light-weight self-contained unit suitable for use in field-mapping experiments. These considerations led to the present design which uses a 6 in. radial stub antenna mounted on an aluminum sphere 25 in. in diameter. The recording instrumentation includes an oscilloscope, a 35-mm camera, and a battery power source, all of which are contained within the spherical shell. The total weight of the instrument is 50 lb.

When exposed to an incident plane-wave E_0, the radial electric field at the surface of the sphere is given by[4]

$$E_r = \frac{-E_0 \cos\theta}{(ka)^2} \sum_{n=1}^{\infty} j^{-n}(2n+1) \frac{P_n'(\cos\theta)}{h_n^{(2)}(ka) + (ka)h_n^{(2)'}(ka)}, \quad (1)$$

where $h_n^{(2)}(ka)$ is the spherical Hankel function and the prime denotes its derivative with respect to its argument; $P_n'(\cos\theta)$ is the Associated Legendre Polynomial; k is the free space propagation constant ($k = 2\pi/\lambda$); and a is the radius of the sphere. The geometry is shown in Fig. 3 with the direction of wave propagation along the z axis and the electric field in the x direction. With the stub antenna located at $r = a$, $\theta = \pi/2$, $\phi = 0$, the angle $\phi = \pi/2 - \theta$ corresponds to the elevation angle measured from the sphere to the source point. For $ka \ll 1$, Eq. (1) reduces to the static field solution

$$E(r) = 1 + \frac{2a^3}{r^3} E_0 \cos\theta \quad (2)$$

evaluated at $r = a$.

The magnitude $|E/E_0|$ from Eq. (1) is plotted in Fig. 4 as a function of elevation angle for frequencies between 20 and 100 MHz. The static field solution is included for comparison. The curves show the static field solution to be within 10% of the full solution for frequencies below approximately 80 MHz at elevation angles between +6° and -30°.

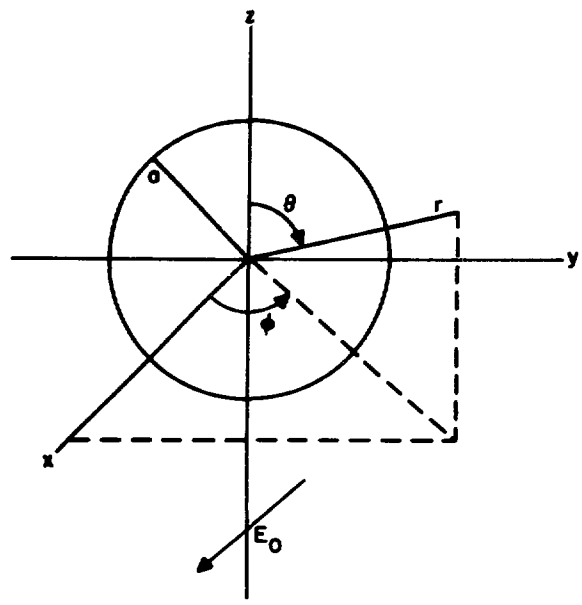

Fig. 3
Geometry of sphere.

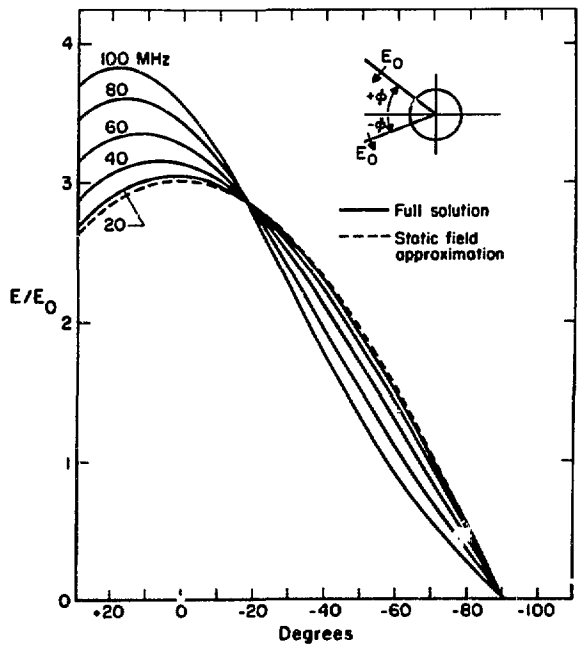

Fig 4
Radiation pattern of a dipole on a sphere.

The effective height of the stub antenna of length L is given by the integral

$$h_e = \frac{1}{I_0}\int_a^{a+L} I(r) \times E(r)dr \ . \qquad (3)$$

Using the static field solution for E(r) and a linear current distribution for I(r) gives

$$h_e = \frac{L}{2}\left(1 + \frac{2}{1 + L/a}\right) \qquad (4)$$

for the effective height of a short probe mounted on a spherical surface. Since L/2 is the effective height of a short probe mounted on a flat ground plane, the quantity in parenthesis can be interpreted as a curvature factor which accounts for the increase of the radial electric field near the curved surface of the sphere. With L = 6 in. and a = 12.5 in., the antenna effective height and curvature factor are 0.18 m and 2.35, respectively.

The antenna equivalent circuit is shown in Fig. 5. The antenna and load impedances Z_A and Z_B form a voltage divider which reduces the sensor sensitivity by an amount $Z_A/(Z_A + Z_3)$. The resultant sensitivity in volts per volt/meter is then

$$V_L/E = h_e Z_A/(Z_A + Z_B) \ .$$

In practice, the impedances Z_A and Z_B are capacitive and can be measured separately. However, to eliminate possible errors that might occur in the separate determination of Z_A and Z_B, the sensor was calibrated experimentally. Measurements were made on a 1/4-scale model of the sphere using the parallel plate transmission line facility at LASL. The facility produces a uniform field that is known to an accuracy of 1%. The resultant sensitivity of the sensor was found to be 7.5×10^{-4} V per V/m when loaded with a 100:1 scope probe (Tektronix Model P6009).

The transmission line facility was also used to verify the curvature factor. Measurements were made with the 1/4-scale probe mounted on a flat ground plane and on a 6-in.-diam sphere. The measured curvature factor was found to be 2.42, in good agreement with the calculated value of 2.35. The results verify that the assumptions made in deriving Eq. (4), i.e., a linear current distribution and use of the static rather than the full-field solution, are valid assumptions.

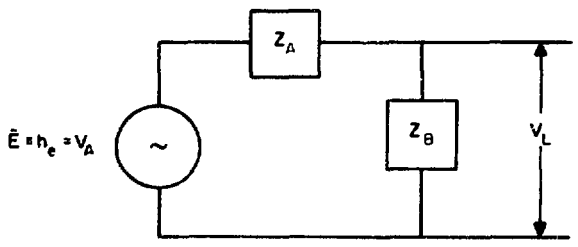

Fig. 5
Antenna equivalent circuit.

IV. DATA ANALYSIS

A printout of aircraft position and attitude was made at 5-sec intervals during the time pulses were transmitted from the simulator. World time to the nearest second was simultaneously recorded with the position data. The slant range, azimuth, and depression angle was manually recorded at pulse time from a precision radar. World time was also recorded on the 35-mm film for both BA sensors and the AD sensor.

Assuming film speed to be constant, actual pulse time was measured to the nearest millisecond. The position and attitude of the aircraft was then linearly interpolated for the actual pulse time. The slant range from the precision radar was undoubtedly more accurate than the position information from the inertial guidance system (INS). The radar information was manually recorded while the INS information was automatically recorded at precise intervals. A graphic analysis of aircraft position with respect to time demonstrated that INS position was more reliable for individual readings. Since the INS is subject to drift, the precision radar information will be automatically recorded and used in future experiments of this type.

Close-in sensor information was identified by pulse number and clock time. Aircraft sensor information was identified by digital time on the edge of the film. After the film was processed, it was readily marked by pulse number. The data pulses, with time and amplitude calibrations, were read and cards punched in microns vs microns. For the data pulses, the cards also contained tags to indicate the beginning and the top of the first peaks to facilitate rapid calculations of the peak amplitudes.

Volts vs time for the data pulses was obtained by linear interpolation of the calibration data. Amplitudes for the pulses were calculated in volts/meter and, using the slant range, were calculated in volts/meter at 1 km.

To obtain graphs in the frequency domain, a fast Fourier transform for real data, written by B. R. Hunt of LASL, based on the method of Singleton,[5] was used.

Amplitudes of the aircraft data were multiplied by the ratio of the first-peak amplitude of the aircraft sensor to the first-peak amplitude of the sphere sensor. The aircraft traces were then subtracted from the sphere traces to obtain the residue, which was plotted in both the time and frequency domain.

V. RESULTS

Discounting aircraft reflections, particularly those from the wing tips,[6,7] the difference in time between the first maximum positive peak and the maximum negative peak was seen to be significantly longer for the BA and shorter for the AD than that measured for the close-in sensors. This is assumed to be caused by the phase-distortion of the free-space field by the aircraft structure. This distortion could be cosine-related to the free-space field. It was found that the BA time multiplied by the lobe correction, and the AD time divided by the lobe correction, gave a value very close to that of the DRI sphere. The reason for this may be coincidental, but it is believed to have some physical relationship, unexplained at this time. Some of this effect could be propagation delay in the atmosphere although it does not appear to agree well with published information, for example, Levine (1970).[8] Of the 55 pulses studied, pulse 15 of 10/24/72 is used as a typical example. Time and frequency domain plots are shown as Figs. 6 through 17 after all the corrections above had been applied.

The enhancement factor (E_f) on effective antenna and sensor system gain was then calculated by dividing the first maximum normalized and corrected peak on the aircraft by the value of the normalized and corrected same peak from the sphere sensor. This was then examined with respect to the depression angle of the simulator from the aircraft, the azimuth angle of the simulator from the aircraft, and the elevation angle of the aircraft from the simulator. These relationships are plotted in Figs. 18 through 28. Some variational trend can be seen, particularly when the ray path passes near the wing tip. If the azimuth angle is limited to ± 2% from the beam, and the depression angle from 8° to 12°, then the E_f for the BA is 2.18 ± 13% and for the AD is 1.28 ± 14%. No correlation between roll angle and E_f was

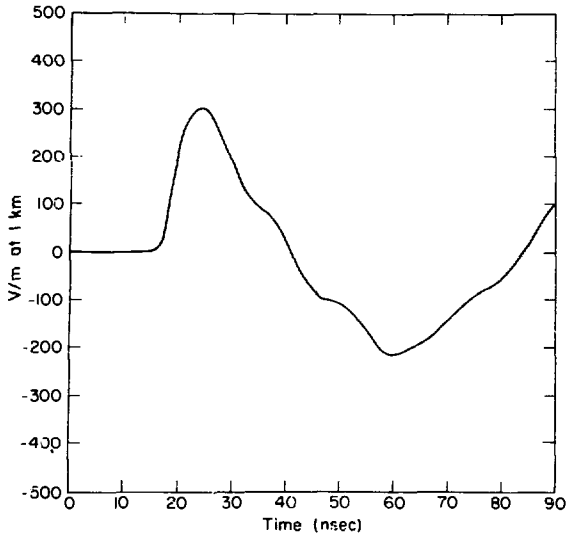

Fig. 7
B sensor. Trace 15 of 10/24/72.

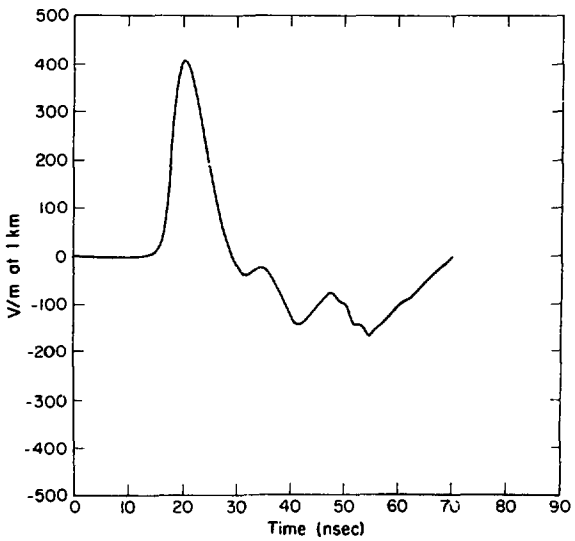

Fig. 6
Sphere sensor. Trace 15 of 10/24/72.

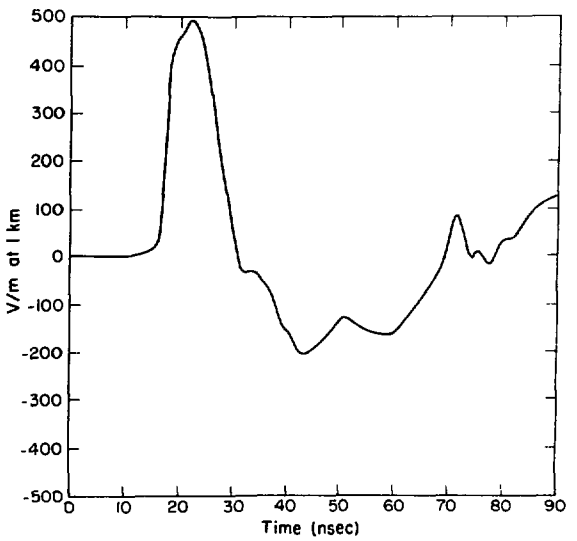

Fig. 8
$\bar{E}$ sensor. Trace 15 of 10/24/72.

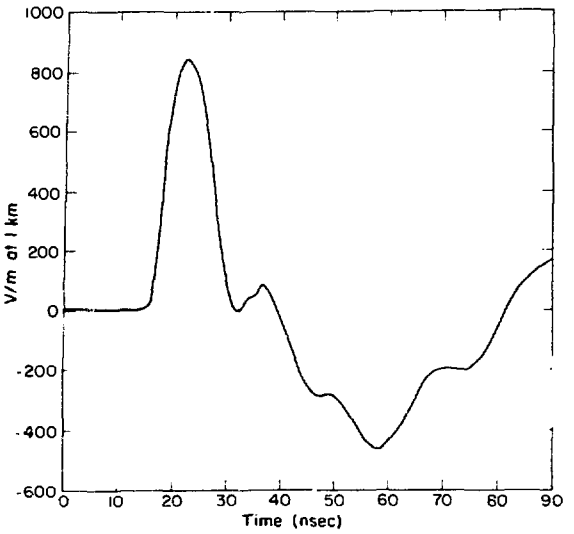

Fig. 9
BA sensor scope 1. Trace 15 of 10/24/72.

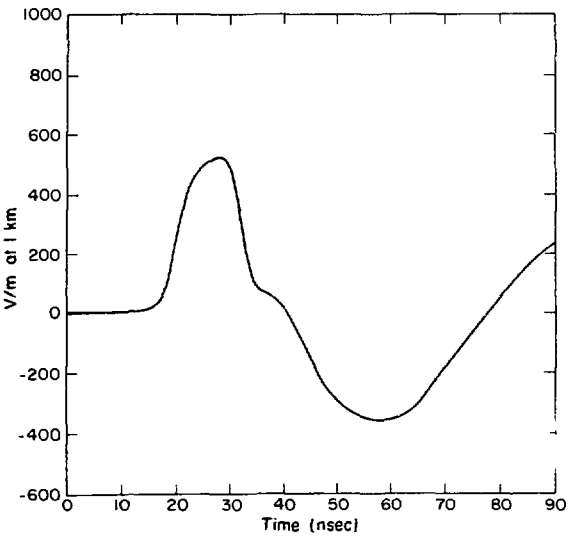

Fig. 11
AD sensor. Trace 15 of 10/24/72.

observed. Table 1 lists E_f for the average corrected reading from the BA, and for the AD vs azimuth and depression angles for 29 pulses.

CONCLUSIONS

For any type of EMP sensor on any type of aircraft, there exists an enhancement factor which shows significant variation in time and amplitude from that of the free space field. For any specific system, a factor of three or so may be measured over a relatively small variation of azimuth and depression angles. Because of the geometry of an individual aircraft, the location of an EMP sensor on the aircraft, and the charge distribution on the aircraft due to an EMP signal, it is difficult if not impossible to

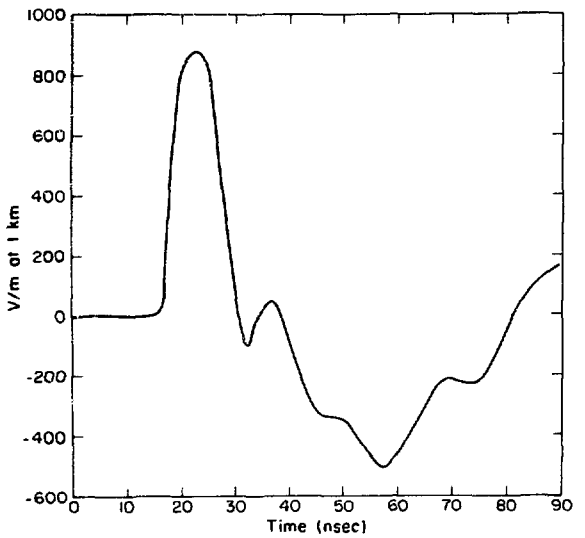

Fig. 10
BA sensor scope 2. Trace 15 of 10/24/72.

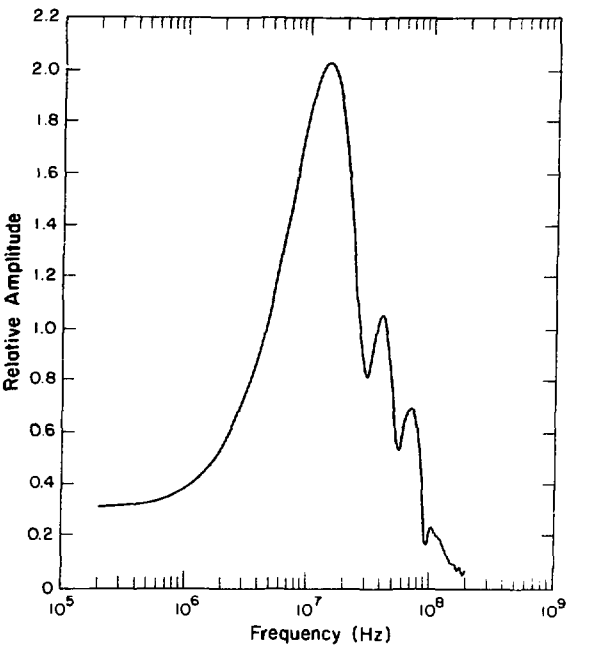

Fig. 12
Sphere sensor. Trace 15 of 10/24/72.

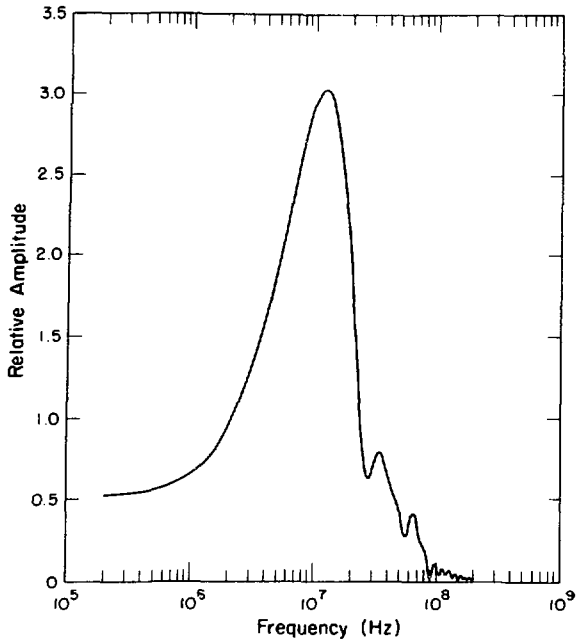

Fig. 13
$\dot{B}$ sensor. Trace 15 of 10/24/72.

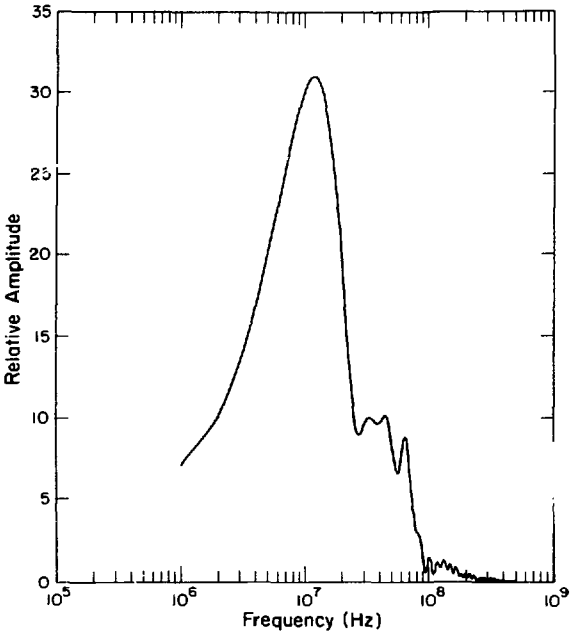

Fig. 15
BA sensor scope 1. Trace 15 of 10/24/72.

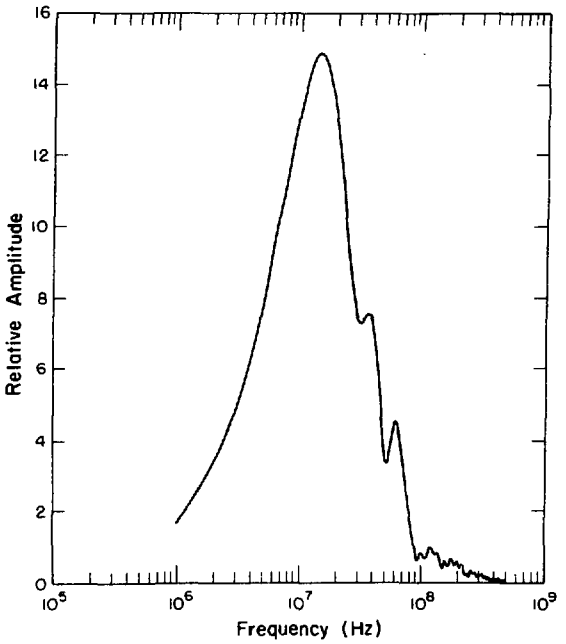

Fig. 14
$\overline{E}$ sensor. Trace 15 of 10/24/72.

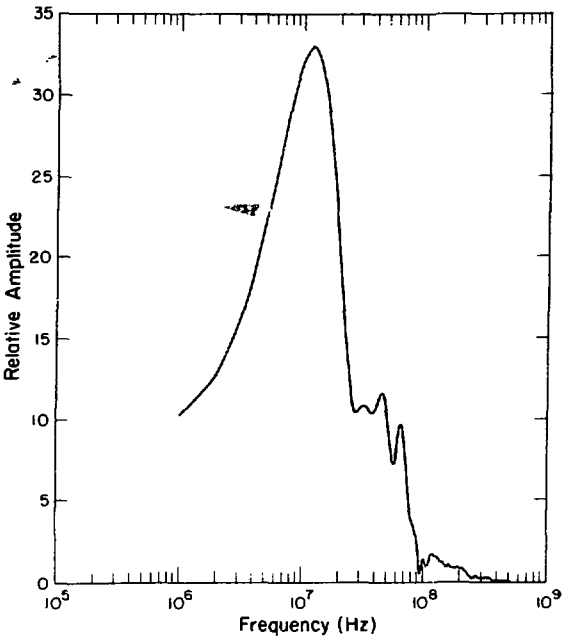

Fig. 16
BA sensor scope 2. Trace 15 of 10/24/72.

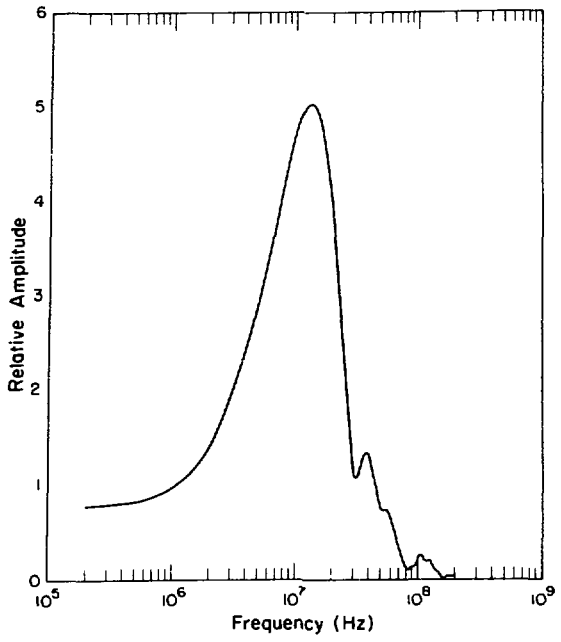

Fig. 17
AD sensor. Trace 15 of 10/24/72.

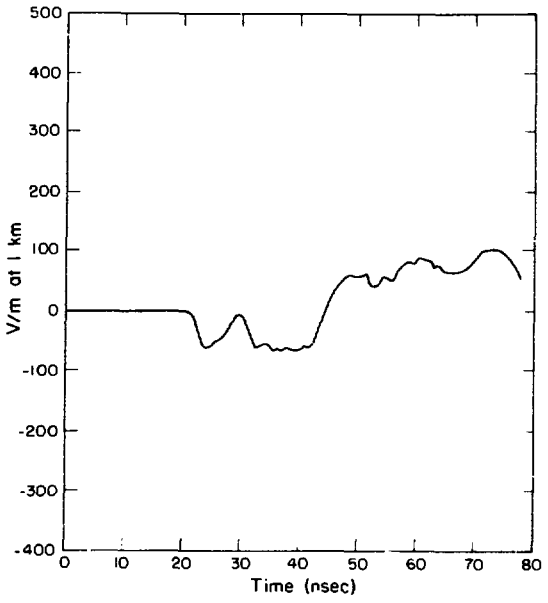

Fig. 19
Sphere sensor minus BA sensor, lobe and E_f corrected. Trace 15 of 10/24/72.

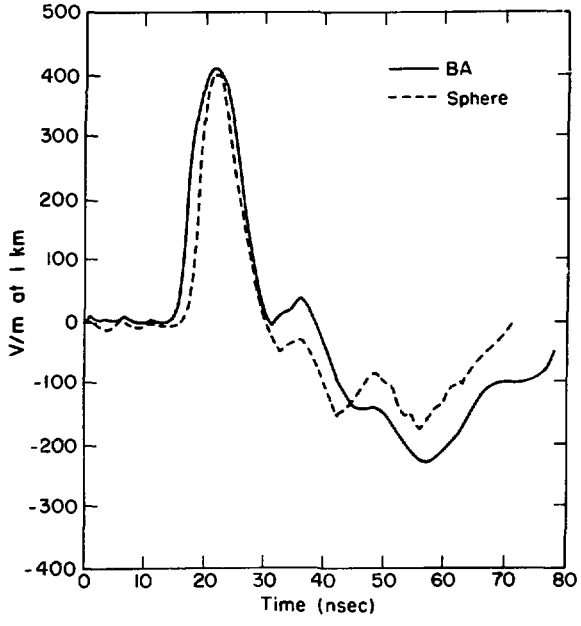

Fig. 18
Sphere and BA sensors, lobe and E_f corrected. Trace 15 of 10/24/72.

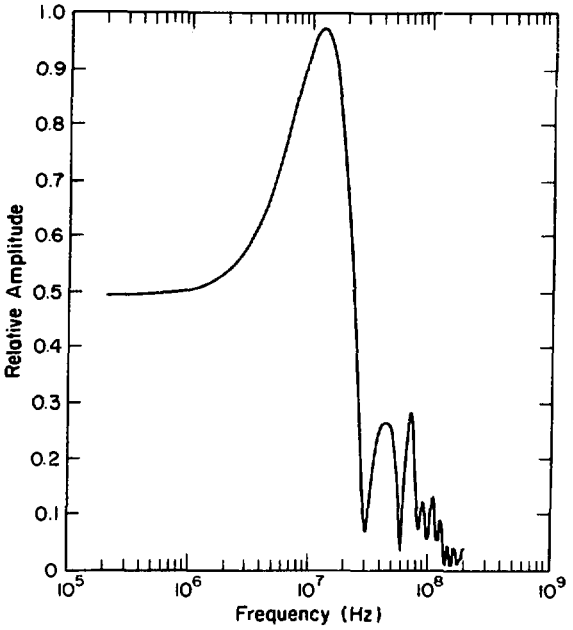

Fig. 20.
Sphere minus BA sensor. Trace 15 of 10/24/72.

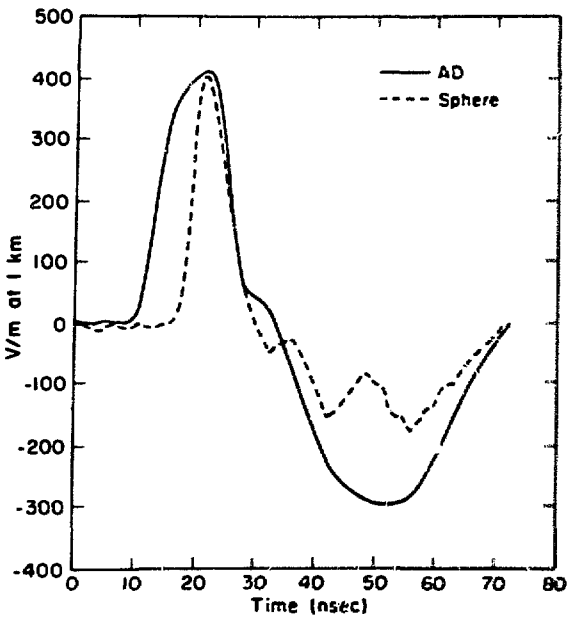

Fig. 21
Sphere and AD sensors, lobe and E_f corrected. Trace 15 of 10/24/72.

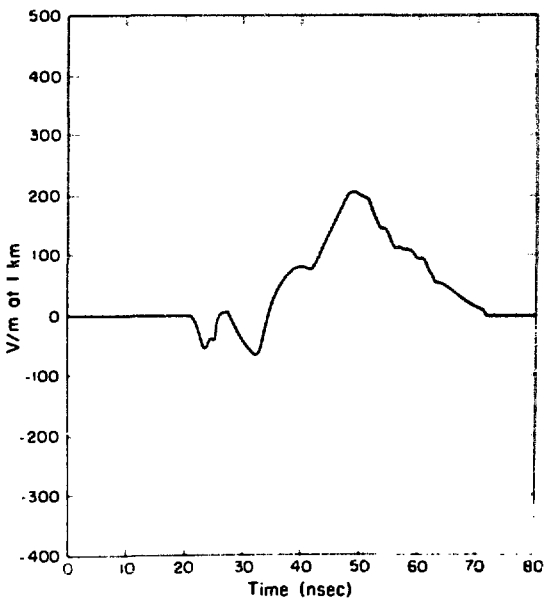

Fig. 22.
Sphere minus AD sensor, lobe and E_f corrected. Trace 15 of 10/24/72.

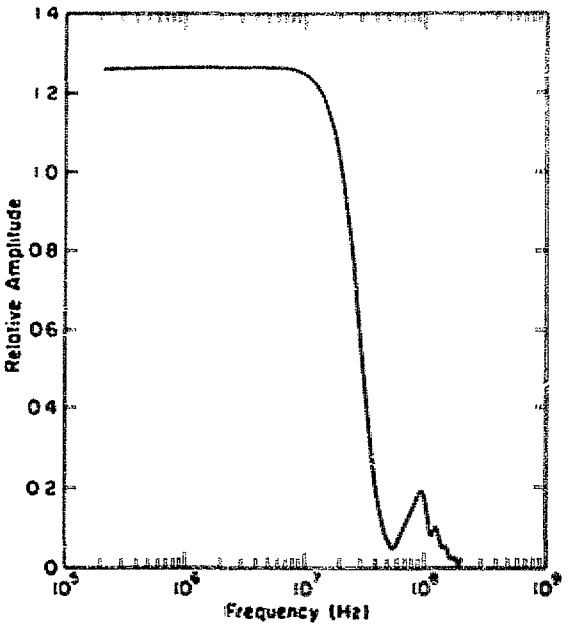

Fig. 23
Sphere minus AD sensor, lobe and E_f corrected. Trace 15 of 10/24/72.

calculate precisely the E_f for an EMP sensor on the aircraft. It is believed that the E_f can be measured to about ± 5% under carefully controlled conditions however.

The required conditions for precise measurement of E_f are as follows:

1. Aircraft position, heading, pitch, roll, and attitude must be automatically recorded every 5 sec using the best available means, at least for three readings before and after the actual pulse.

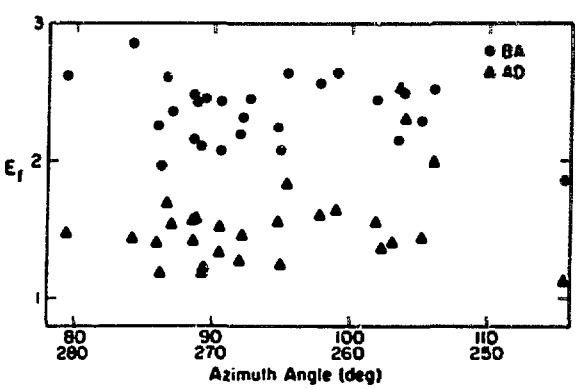

Fig. 24
E_f vs azimuth.

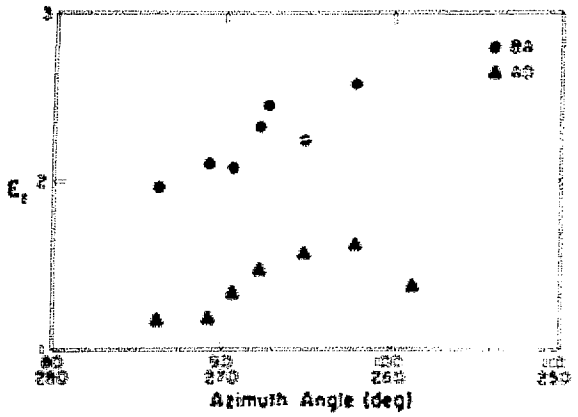

Fig. 25
E_f vs azimuth for 8° to 11° depression angles.

2. The radiated pattern from the pulser in azimuth and elevation must be well known in the direction of the aircraft at pulse time.

3. Close-in measurements must be made at a location close to the ray path and at a sufficient distance so that there is little or no effect from the inductive or static fields for the frequency domain of interest.

4. All sensors involved must be accurately calibrated. It is desirable to have at least two close-in sensors and two independent readings for each aircraft antenna. Each aircraft system must have a complete calibration as installed.

5. Several pulses should be taken under almost identical conditions for a good statistical average.

6. No pulses should be taken (or used) when the ray path from the aircraft to the source passes within ± 1 1/2° from the wing tip (trailing edge or leading edge) for an individual antenna because E_f changes rapidly in this region.

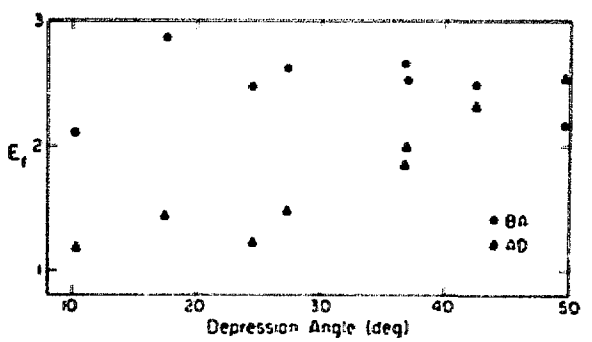

Fig. 26
E_f vs depression angle.

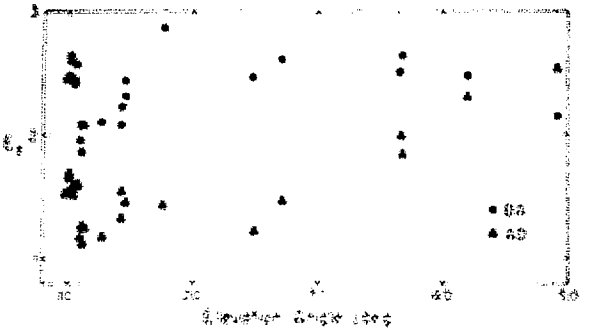

Fig. 27
E_f vs elevation angle.

ACKNOWLEDGEMENTS

The authors wish to acknowledge the support of the agencies and personnel involved in this experiment. We are particularly grateful to W. B. Hills, Director, Pacific Area Support Office of the AEC for his support and assistance in the construction and operation of the simulator and close-in sensors at Hickam Air Force Base. R. L. Wakefield materially contributed in taking the aircraft data and assisted in the preparation of the flight plans. R. E. Partridge of LASL was very helpful in the construction of the close-in parallel $\vec{E}$ plate sensor, overall coordination of ground activities during the experiment, and in the sensor calibration. We are grateful also for the contributions from many people from the Sandia Laboratories, Albuquerque; EG&G, Albuquerque; Holmes and Narver, Honolulu; the Air Force crew which flew the difficult flight plans; and the support personnel from LASL and DKI.

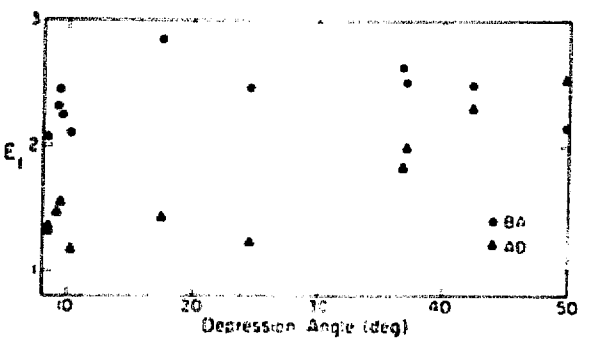

Fig. 28
E_f vs depression angle for 1° forward to 26° aft of beam.

TABLE I

ENHANCEMENT FACTOR WITH RESPECT TO AZIMUTH AND DEPRESSION ANGLE FROM THE AIRCRAFT TO THE SOURCE

Date	Pulse No.	Azimuth (deg)	Depression (deg)	Enhancement Factor BA	Enhancement Factor AD
10/24	10	90.5	8.4	2.1	1.3
	11	92.2	9.1	2.3	1.5
	12	92.7	9.3	2.5	
	13	94.8	9.4	2.2	1.6
	14	273.8	8.0	2.0	1.2
	15	268.0	6.1	2.1	1.3
	16	265.1	5.9	2.1	1.2
	17	244.4	5.9	1.9	1.1
	18	106.1	37.1	2.5	2.0
	19	270.7	24.5	2.5	1.2
	20	103.5	49.7	2.2	2.5
	21	103.9	42.5	2.5	2.3
	22	95.4	36.8	2.7	1.8
	23	275.8	17.5	2.9	1.4
	24	79.3	27.3	2.6	1.5
	25	270.8	10.3	2.1	1.2
10/26	3	102.3	8.1		1.4
	4	103.1	4.8		1.4
	5	88.6	-0.6	2.2	1.4
	6	86.0	7.4	2.3	1.4
	7	87.1	3.2	2.4	1.5
	8	88.6	6.9	2.5	1.6
	9	88.8	7.4	2.4	1.6
	10	90.5	7.3	2.4	1.5
	11	97.9	8.2	2.6	1.6
	12	99.0	7.1	2.7	1.6
	13	101.9	7.1	2.5	1.5
	14	105.3	6.8	2.3	1.4
	17	86.7	-3.5	2.6	1.7

☆ US GOVERNMENT PRINTING OFFICE: 1973 — 784-519/4
CM:401(140)

REFERENCES

1. C. U. Benton, R. L. Wakefield, E. D. Niper, and R. L. Schellenbaum, "EMP in the Ionosphere" Los Alamos Scientific Laboratory, report LA-4947 (September 1972).

2. H. M. Peck and K. N. Joy, "Operation Picaposte," Los Alamos Scientific Laboratory Internal Document (September 1972).

3. R. W. Buchanan, System Response and Propagation Studies, University of Denver, Denver Research Institute, report DRI #2613 (December 1972).

4. R. F. Harrington, Time Harmonic Electromagnetic Fields, McGraw-Hill, p.294, (1961).

5. R. C. Singleton, "On Computing the Fast Fourier Transform," *Comm. ACM*, Vol. 10, 1967, pp. 647-654.

6. R. J. Lytle and D. L. Lager, Electromagnetic Propagation Transmission, Reflection, and Refraction: Equations and Numerical Results, Lawrence Livermore Laboratory, report UCRL-51245 (June 1972).

7. R. R. Lentz, P. H. Pathok, and W. D. Burnside, The Ohio State University Electroscience Laboratory, Interaction Notes, Note 117 (June 1972).

8. D. M. Levine, Propagation Delay in the Atmosphere, NASA report NASA-TM-X-65460 (November 1970).